Composites: Part A 175 (2023) 107755

Contents lists available at ScienceDirect

Composites Part A

journal homepage: www.elsevier.com/locate/compositesa

Dielectric parameter independent curing analysis of out-of-autoclave carbon fibre/epoxy composites

Molly Hall [a,*], Xuesen Zeng [a], Tristan Shelley [a], Peter Schubel [a]

[a] Centre for Future Materials, University of Southern Queensland, Toowoomba, QLD 4350, Australia

ARTICLE INFO

Keywords:
A. Thermosetting resin
B. Cure behaviour
B. Electrical properties
Dielectric sensors

ABSTRACT

Due to their capability to evaluate the microscopic mobility of polymers, dielectric sensors are increasingly used for in-situ cure monitoring of thermoset composites. More than a dozen cure correlation methods have been proposed in literature to date, each of which focuses on a specific dielectric parameter. However, the wide variety of techniques have not been compared nor robustly evaluated for accuracy and repeatability. This study collects dielectric signal data (dissipation factor, impedance, ionic conductivity/viscosity, loss factor, and permittivity) during cure of an out-of-autoclave thermoset prepreg and conducts a systematic evaluation of the five dielectric parameters to prove that the parameters can be used interchangeably and, in some cases, can deliver complementary information. By correlating features of dielectric graphs to both experimentally measured and numerically simulated cure state events, a master list of correlation techniques is presented. The proposed techniques have improved accuracy and repeatability in comparison to the existing analysis techniques.

1. Introduction

Advanced thermoset polymer composites have been implemented by a range of industries due to their combination of excellent properties and wide variety of manufacturing techniques [1–14]. Fibre reinforced polymer (FRP) composites research is currently focused on enabling high quality and high complexity parts [15,16], with much emphasis on optimising the processing conditions for fabrication [17–19]. Composite parts are susceptible to a variety of quality issues due to high levels of manufacturing uncertainty stemming from variation in the raw materials and processing conditions [20,21]. A major challenge in optimising composites processing techniques is accounting for the impact of system variability on the final product output. Quality control requirements commonly dictate that components must achieve a specified state of resin cure, as the completion of the polymer conversion process is directly linked to the mechanical performance of the final product [22]. As the complexity and scale of composite parts increases it becomes more challenging to meet this threshold. Much research is being conducted on using different types of sensors for in-situ cure monitoring as a method of demonstrating compliance to quality requirements. In-situ sensor networks are also an appealing technology for enabling active control of the manufacturing process. By having direct knowledge of the material state, processes parameters can be updated live which allows for process optimisation.

A range of sensor types have been investigated for their ability to monitor this thermoset cure state including thermocouples, ultrasonic sensors [23–25], fibre optic sensors [26–28], and dielectric sensors [29–31]. The capabilities and limitations of these sensors have been extensively reviewed [32,33]. A recent review on these four common in-situ cure monitoring sensors has explored the different methods for correlating monitored parameters to cure state information [34]. Thermocouples monitor the change in temperature, which can then be used as an input to a kinetic model for a given resin system to understand cure state. Ultrasonic sensors monitor the change in attenuation of ultrasonic waves as they propagate through the material, showing clear phase transformations as the matrix crosslinks and changes in density. Fibre optic sensors, depending on the type, will monitor how light refraction or strain changes in response to a cross-linking matrix. Dielectric sensors, however, are one of the most promising methods of in-situ cure monitoring as they have identified not just phase transitions, but degree of cure (DoC) and glass transition temperature (T_g) progression. The reader is encouraged to use this review as a supplement for the brief summary of analysis techniques provided here, and in particular for the current state of the art for dielectric analysis.

The dielectric sensor operates by generating a time varying electric field which fluctuates at a set frequency or range of frequencies.

* Corresponding author.
E-mail address: molly.hall@usq.edu.au (M. Hall).

https://doi.org/10.1016/j.compositesa.2023.107755
Received 1 June 2023; Received in revised form 2 August 2023; Accepted 24 August 2023
Available online 25 August 2023

Dielectric analysis (DEA) is then conducted by monitoring changes in the electrical behaviour of the polymer during cure and relating these events in the electrical behaviour to physical material changes. A current is generated in response to the sensor's applied excitation voltage, which results in a total electrical impedance of the material. This measurement is composed of resistive and capacitive components, which originates from ion movement and dipole rotation within the material under test. As the material cures and the polymer chains crosslink, the ion and dipole movements are restricted. By monitoring these changes as the cure time progresses, it is possible to identify major curing events such as the onset of the cure reaction, point of minimum resin viscosity, and end of the cure reaction.

Many researchers have investigated methods of conducting DEA, however each have used different parameters and methods to correlate dielectric information with material cure state information. Commonly, analysis is completed by evaluating signal change as time progresses (time-spectrum) or signal change across a range of frequencies (frequency-domain) [35–37]. A summary of key time-spectrum analysis techniques is presented in Table 1. This material presented in this study displays frequency-independent behaviour at the investigated frequencies due to the impact of ion migration dominating the dielectric signal [38]. For this reason, this paper will focus on time-spectrum analyses and their correlations with thermodynamic transitions and reactions of the material under test. To date, the existing methods have not been compared side by side to evaluate their accuracy and repeatability. This paper presents a systematic approach to correlating dielectric signals to material cure state information for the cure of Solvay CYCOM® 5320-1 carbon fibre/epoxy prepreg. Cure characterisation for 5320-1 has been completed by [39] and further refined by [40]. The kinetic model used here, via Convergent RAVEN, is based on the Kratz model [39]. A thorough evaluation is presented for multiple cures, with consideration of all dielectric parameters and their correlations to simulated and analytical test results. As all five dielectric parameters are calculated based on the materials' dielectric behaviour, specifically capacitive and resistive response, this paper hypothesises that the dielectric parameters can be used interchangeably for the monitoring of thermoset cure reactions. Based on this, a final set of correlation techniques is proposed, including validation and verification of existing techniques and proposed modifications and updates for future implementation.

Table 1
Overview of existing dielectric correlation methods, including the method used and the cure feature that is output from the method. Methods are indicated by the dielectric parameter with DISP indicating the dissipation factor (D), IMP indicating the Impedance (Z), COND indicating the ion conductivity (σ), LOSS indicating the loss factor (ε''), and VISC indicating the ion viscosity (ρ).

Name	Method	Cure Feature	Sources
DISP-1	First local maximum of $\frac{dD}{dt}$	Cure start	[47]
DISP-2	Plateau onset ($\frac{dD}{dt} = 0$)	Cure completion	[47]
DISP-3	tanδ = 1 defined as the crossover point between loss and permittivity	Gel point	[49]
IMP-1	Onset of the first plateau after the minimum value of impedance at 1 kHz	Gel point	[30,45]
IMP-2	Onset of the second plateau after the minimum value of impedance at 1 kHz	Vitrification	[30,45]
IMP-3	Linear regression to determine relationship between log(Impedance) and degree of cure over the isothermal range	Degree of cure progression	[52]
COND-1	Global maximum of the conductivity	Minimum viscosity	[31,53]
COND-2	Inflection after the peak of the conductivity	First indication of gelled material	[31,53]
COND-3	Plateau onset ($\frac{d\sigma}{dt} = 0$)	Vitrification	[31,53]
COND-4	$T_g = \frac{\log\sigma_0 - \log\sigma_t}{\log\sigma_0 - \log\sigma_\infty} T_{g\infty}$ With the conductivity at the start (σ_0) and end (σ_∞) of the isothermal region, conductivity at time t (σ_t), and the measured glass transition temperature ($T_{g\infty}$)	T_g progression	[46]
LOSS-1	$\alpha = \frac{\log\varepsilon''_0 - \log\varepsilon''_t}{\log\varepsilon''_0 - \log\varepsilon''_\infty}$ With the loss factor at the start (ε''_0) and end (ε''_∞) of the isothermal region, and the loss factor at time t (ε''_t).	Cure index	[54]
VISC-1	Plateau onset ($\frac{d\rho}{dt} = 0$)	Cure completion	[48,55]
VISC-2	$\alpha = \frac{\log\rho_t - \log\rho_{min}}{\log\rho_{max} - \log\rho_{min}} \alpha_m$ With the viscosity at time t (ρ_t), minimum viscosity (ρ_{min}), maximum viscosity (ρ_{max}), and the measured degree of cure (α_m)	Degree of cure progression	[30]

2. Methodology

2.1. Materials and sample preparation

This study used Solvay CYCOM® 5320-1 carbon fibre/epoxy prepreg, for which the material definition is stated in Table 2. Prepreg squares measuring 80 mm by 80 mm were laid up in a $[0,90]_s$ configuration, with a NETZSCH IDEX 115/60T interdigitated dielectric sensor and a K-type thermocouple embedded at the midplane as shown in Fig. 1. The four-ply configuration was chosen to ensure good contact between the sensor and the epoxy. It should be noted that the sensor has a penetration depth of 115 μm, which is within the first ply placed above the electrodes. Additional thermocouples collected thermal data on the top of the vacuum bag, under the tool, and in the air approximately 100 mm above the top of the bag. A secondary panel, also 80 mm by 80 mm, with layup scheme $[0/90]_{4s}$ was manufactured without any embedded sensors to produce Dynamic Mechanical Analysis (DMA) test specimens. This layup sequence was chosen in accordance with the ASTM standard for DMA testing of composites [41]. Both laminates were fabricated on a 15 mm thick steel tool and vacuum bagged in accordance with the manufacturers recommended vacuum bagging schematic [42]. Five replicates of this assembly, designated IDEX1 through IDEX5, were cured in an oven under vacuum using a modified version of the manufacturers recommended cure cycle. The cure profile started from ambient conditions and increased at 2–2.5 °C/min to 180 °C, followed by a 2-hour dwell at 180 °C, and subsequent cooling back to ambient temperatures. The data collected from these panels follows the data flow indicated in Fig. 2. The following sections detail the methods used to complete the dielectric analysis, cure simulation, and analytical testing.

2.2. RAVEN simulation

Convergent RAVEN software was used to simulate the cure of the prepreg based on the temperature profile collected from the mid-plane thermocouple. This thermocouple was selected for simulation as it corresponds to the location of the embedded IDEX sensor. A 0D cure profile was run using the built-in material card for the CYCOM® 5320-1/IM7-12K Tape based on the Kratz cure kinetics model [39] and using the thermocouple data taken from the midplane of the laminate. Cure

Table 2
Solvay CYCOM® 5320-1 prepreg definition and properties [42].

Property	Value
Resin	CYCOM® 5320-1
Fibre	Hexcel IM7 12 K
Prepreg Areal Weight (gsm)	145
Resin Content (%)	33
Form	Unidirectional Tape

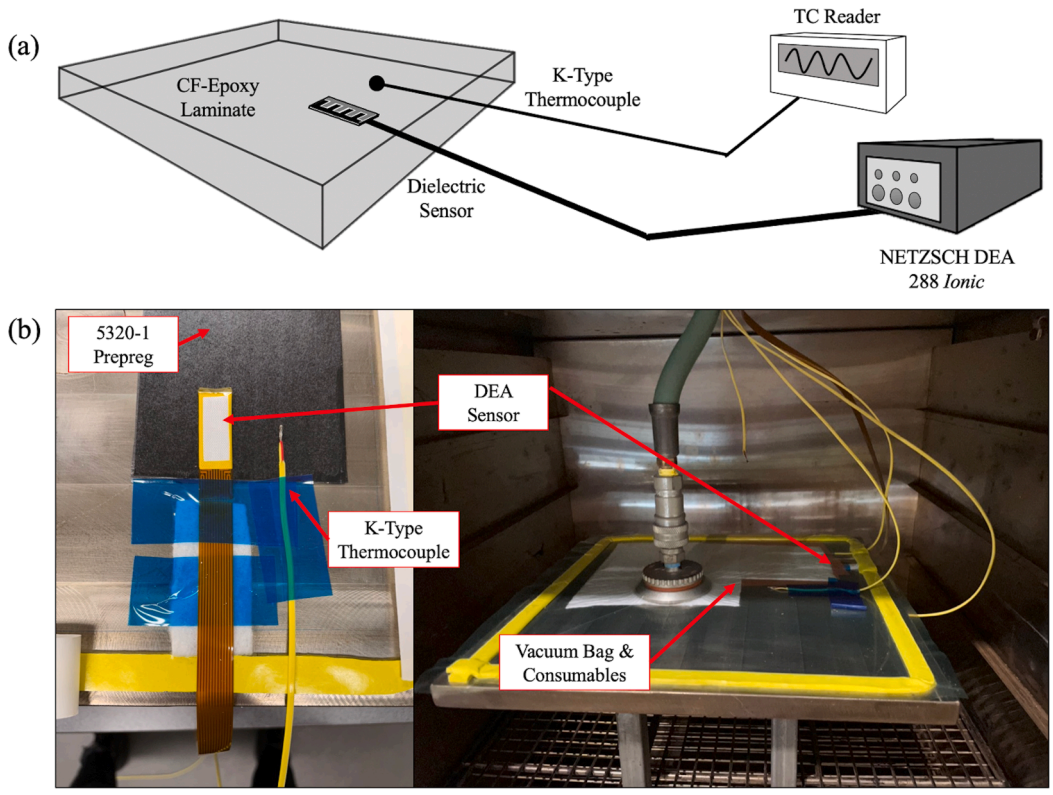

Fig. 1. Cure setup including (a) schematic of sensor placement within the midplane of the laminate and (b) image of sensor placement within the laminate and laminate placement within the oven. Note that placement of TC Reader and DEA Reader shown in (a) are located outside of the oven.

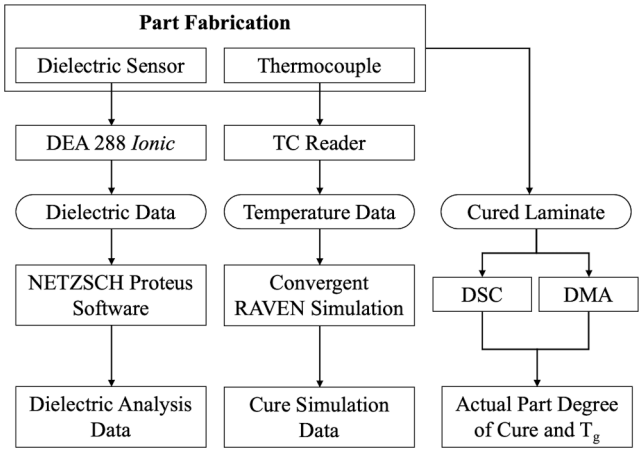

Fig. 2. Schematic of data flow from data collection to analysis.

features were identified for each IDEX panel in accordance with Fig. 3. The final degree of cure shown in (a) is identified as the end value of the degree of cure curve. The vitrification point shown in (b) is identified as the crossover point between the T_g and temperature, and the final T_g also shown in (b) is identified as the end value of the T_g curve. The start of cure and end of cure both found in (c) is indicated by the start and ending of the cure reaction rate. The time at minimum viscosity shown in (d) is indicated by the global minimum, and the gel point also shown in (d) is indicated by the inflection of the viscosity curve. The logarithmic scale for (d) should be noted.

2.3. DSC measurements

Differential Scanning Calorimetry (DSC) was conducted using a TA DSC25. Approximately 5–10 mg of material cut from each IDEX panel was tested under a dynamic ramp rate of 5 °C/min from 25 to 280 °C. The actual laminate degree of cure was calculated by integrating under the heat flow-time curve and dividing by the total heat of reaction for 5320-1, which is indicated as 561.8 J/g per Convergent RAVEN.

2.4. DMA measurements

Dynamic Mechanical Analysis (DMA) was conducted using a TA HR-2 Hybrid Rheometer. Test coupons were cut by waterjet from the $[0/90]_{4s}$ panel to dimensions of 8 mm wide by 45 mm long with a tolerance of ±2 mm. They were dried in an air circulated oven at 120 °C for a minimum of 16 h, and then held in a sealed container with desiccant prior to testing. They were tested by a dynamic ramp rate of 5 °C/min from 25 to 280 °C with a displacement of 50 μm oscillating at 1 Hz frequency. The T_g was calculated in accordance with ASTM D 7028 [41] by the storage modulus (E') onset, and the degree of cure was calculated using this value and the DiBenedetto equation.

2.5. Dielectric analysis

2.5.1. Data collection

Dielectric data was collected using NETZSCH IDEX 115/60T interdigitated sensors and the NETZSCH DEA 288 *Ionic* data analyser. The sensor collected parameter data for frequencies between 1 Hz and 10 kHz with 4 frequencies set logarithmically per decade. The resistive (R) and capacitive (C) responses of the material under the time varying electric field were used to calculate the five dielectric parameters.

The complex permittivity (ε^*) is a measure of the polarizability of a material under a time-varying electric field. It is composed of a relative permittivity (ε') calculated via Equation (1) and a loss component (ε'') calculated by Equation (2) [43].

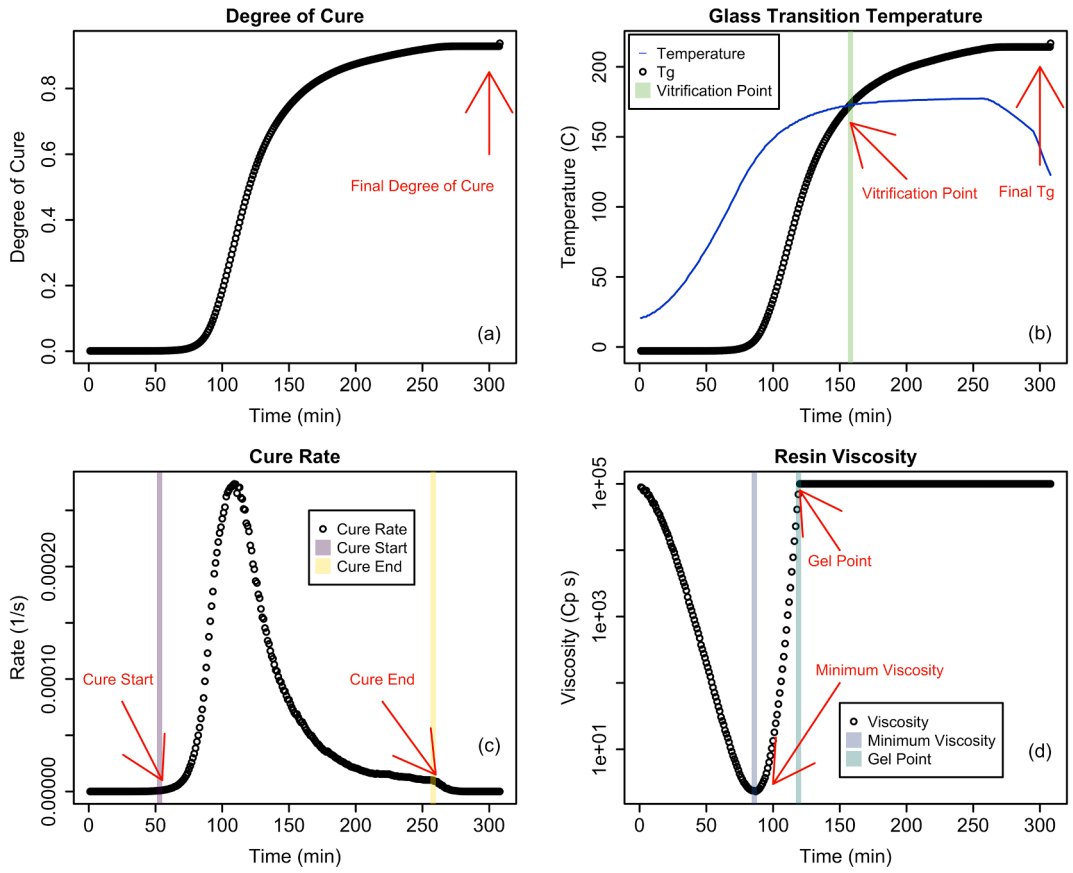

Fig. 3. Method of determining cure states using Convergent RAVEN, indicated with red arrows. (For interpretation of the references to colour in this figure legend, the reader is referred to the web version of this article.)

$$\varepsilon' = \frac{Cd}{\varepsilon_0 A} \tag{1}$$

$$\varepsilon'' = \frac{d}{R\omega A\varepsilon_0} \tag{2}$$

The dissipation factor (D), also known as $tan\delta$, can be calculated in Equation (3) as the ratio of the dielectric loss (loss component) and permittivity (storage component) [44]:

$$D = \tan\delta = \frac{\varepsilon''}{\varepsilon'} = \frac{1}{\omega RC} \tag{3}$$

The ionic conductivity (σ) is a material property related to the bulk dielectric conductance (G), which is the inverse of the resistance (R). It is also related to the ion viscosity (ρ) by an inverse relationship demonstrated in Equation (4) [37]. It should be noted that the ion viscosity is a term which is used to represent the frequency independent resistivity (ρ_{DC}), which here will be represented as ρ for simplicity. Within dielectric analysis it is common to represent the log of the ionic conductivity, which is referred to as the LIC.

$$\rho = \frac{1}{\sigma} = \frac{RA}{d} \tag{4}$$

Impedance (Z) is calculated in Equation (5) with i representing the complex number [37].

$$Z = \frac{1}{\frac{1}{R} + i\omega C} \tag{5}$$

Equations (1)–(5) utilise the shape factor (A/d) driven by the electrode spacing and sensing area, permittivity of free space ($\varepsilon_0 = 8.854 \times 10^{-12}$ F m^{-1}), and electrical excitation frequency (ω). It should be noted that the shape factor is commonly applied to a parallel plate configuration, however it has been documented to be a relevant scaling factor for other configurations such as interdigitated electrodes, as are used in this paper.

Logarithmic scaling is commonly used for all dielectric parameters to isolate the effects of ion mobility and dipole rotation. For example, the permittivity represented in log scale takes the format of Equation (6). This allows for the separation of the capacitance from the constant variables which do not impact the curing: the electrode $\frac{A}{d}$ ratio and the permittivity of free space. By evaluating the logarithm of the dielectric parameters, the direct impact of curing on the capacitance and resistivity can be isolated.

$$\log\varepsilon' = \log\frac{Cd}{\varepsilon_0 A} = \log C + \log\frac{d}{\varepsilon_0 A} \tag{6}$$

Data was processed using NETZSCH Proteus® software. Signals were smoothed up to software setting 6–8 to minimise signal noise. Data collected at a frequency of 1 Hz was used for all correlations, excepting all dissipation factor methods and IMP-1 and -2, as it most appropriately fits the timescale of the cure reaction for this out-of-autoclave epoxy. It should be noted that resin systems which cure more quickly, in the manner of minutes or seconds, may benefit from higher frequency measurements in order to accurately capture the cure events. Higher frequencies showed significant signal noise, and sufficient smoothing of these curves reduced the accuracy of the measurement. 1 Hz measurements generally had the best resolution and required minimal smoothing of the signal. As this material system displays a strong, frequency-independent conductive behaviour it is acceptable to perform the analyses on a single frequency. Cure state correlations on IDEX3 were repeated for 10 Hz, 100 Hz, and 1 kHz frequencies to verify that the results are aligned with 1 Hz measurements. It was confirmed that the choice of frequency for these methods does not impact the results. The 1

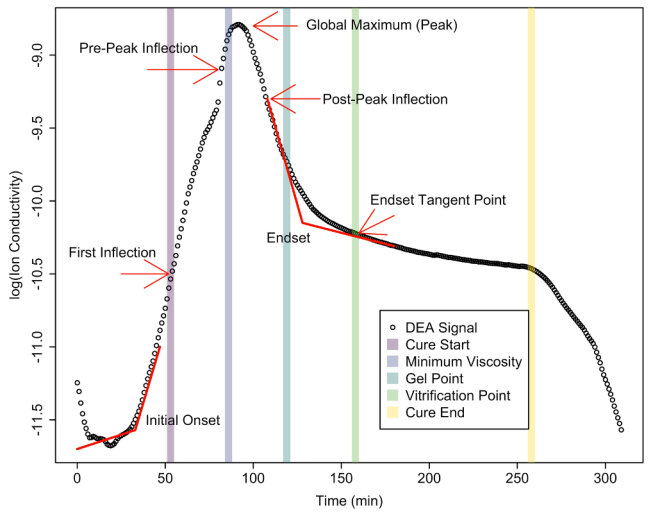

Fig. 4. Identifications of graph features and their placement relative to the RAVEN identified cure events.

Hz frequency was deemed inappropriate for the dissipation factor as it did not have reliable behaviour at low frequencies. Below 100 Hz the signal produced a double peak shape, which distorted the application of the analysis methods. Thus the 100 Hz frequency was selected for the dissipation factor to ensure that the methods can be applied as defined. Finally, the definition of IMP-1 and -2 provided by [30,45] specified the use of 1 kHz measurements, in which it is speculated that the high frequency allows for detection of molecular phenomena. In this study, frequencies between 1 and 3.16 kHz were selected in order to identify the double-shoulder behaviour most clearly.

Data analysis was conducted in accordance with the following sections. A comparison was conducted between the newly proposed correlations, existing correlations, and expansion of the existing correlations to include all dielectric parameters.

2.5.2. *Proposed cure state identification methods*

A cure point analysis was conducted to correlate graph features for each dielectric parameter with cure events defined by the RAVEN simulation. The change in the electrical signals indicates changes in polymer crosslinking, which can therefore be used to indicate the distinct "cure events" which occur during processing: start of cure, minimum resin viscosity, gel point, vitrification point, and the end of cure.

For this analysis, the timing of these cure events was identified from the RAVEN simulation in accordance with the criteria specified in Fig. 3. Similarly, the time at which key dielectric signal changes occurred was identified. These points are known as graph features, and includes inflections, global and local minima and maxima, onsets, endsets, and the point at which the endset intersects the curve (known as the endset tangent). An example of how these graph features are identified is shown in Fig. 4. It should be noted that the impedance follows a concave up graphical trend, whereas all other parameters are concave down. For this reason, the impedance will be referred to using minima where the other parameters will indicate a maximum. The minimum absolute value point of the derivative was used to compare with the end of cure. This point was found by identifying the time at which the minimum absolute value of the derivative curve occurs after the global maximum.

Next, the RAVEN cure events were compared with the dielectric graph features to identify which features correlated most strongly. A preliminary visual comparison, Fig. 5, was conducted to identify which graph features should be considered for comparison. This comparison

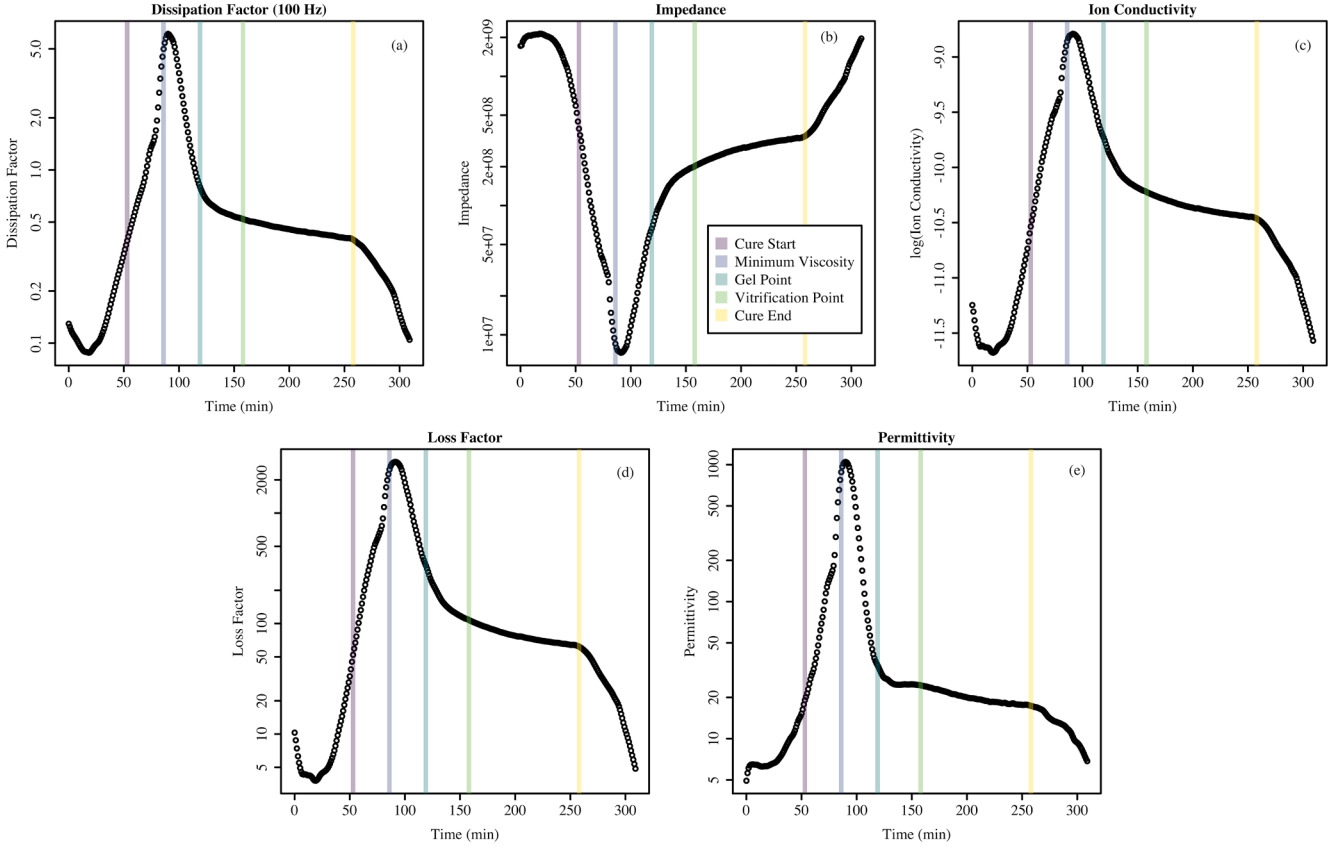

Fig. 5. Comparison of RAVEN cure events (coloured lines) to dielectric signals for (a) Dissipation Factor at 100 Hz frequency, (b) Impedance, (c) Log of the Ionic Conductivity, (d) Loss Factor and (e) Permittivity. Graphs (b-e) represent 1 Hz frequency measurements.

allowed for a down-selection of cure event-graph feature pairs. For some cure events there are multiple graph features which have a potentially strong correlation. For example, the minimum viscosity is located near both the inflection prior to the global maximum, and to the global maximum itself. Both graph feature pairs were identified for the cure point analysis to identify which of them has the strongest correlation amongst all five test replicates. It should be noted that the 100 Hz measurement for the dissipation factor was used for this analysis as it displays a single peak behaviour which most similarly aligns with the behaviour of the other parameters.

The measure of discrepancy strength for each pair was calculated as a percentage of how close the graph feature is to the cure event using Equation (7).

$$\Delta\% = \left| 100 * \frac{(t_{RAVEN} - t_{DEA})}{t_{TOTAL}} \right| \tag{7}$$

The strength (Δ%) was calculated using the time differential between when the RAVEN cure event occurs (t_{RAVEN}) and when the dielectric graph feature occurs (t_{DEA}). It is then normalised by the overall cure time (t_{TOTAL}), which in this case refers to the RAVEN estimated cure end time, in order to scale the results with the duration of the cure. The values and average values are reported as absolute values. This discrepancy rating was calculated for each dielectric parameter, for each pair, for each test replicate (IDEX1-5).

2.5.3. Further development of published cure state identification methods

Many existing DEA correlations have been proposed in literature, however each method specifically identifies a single dielectric variable. These correlations, which are listed in Table 1 are named for the parameter which was originally evaluated. For example, COND-4 proposed by Yang et al. [46] uses the log of the ionic conductivity (LIC) to calculate the progression of the glass transition temperature. Similarly, DISP-1 and DISP-2 which were proposed by Kim et al. [47] identify the start and end of cure by identifying features of the graph of the dissipation factor. This paper evaluates all of the methods proposed in Table 1 for a single material and compares their results across five test replicates. Further, each method was applied across all five dielectric parameters to identify if the method is parameter-dependent.

Developments have been made to some of the existing methods to account for differences in the data structure or as a proposed clarification of the original method. Redefintion or clarifications are detailed below and are summarised for conciseness in Table 3.

- **DISP-2 Redefintion**: DISP-2 identifies the completion of cure as the time where the dissipation factor derivative reaches zero. However, in this study, the derivatives approach zero but never reach it, as cure is stopped prior to the degree of cure reaching 100%. Instead the correlation will define the end of cure, meaning the point where the cure reaction stops, as the minimum of the absolute value of the derivative.
- **DISP-3 Clarification**: DISP-3 was only analysed for the dissipation factor and not implemented for the remaining dielectric parameters as the dissipation factor is specifically a ratio of the loss factor and the permittivity.
- **IMP-1 and IMP-2 Frequency Redefinition**: IMP-1 and IMP-2 were originally identified as the start of two plateau regions identified for the impedance at 1 kHz frequencies. In this study, the double plateau phenomena was only observed at 1 kHz frequencies for IDEX 1 and IDEX5. IDEX3 was most clearly identified at 1.78 kHz, and IDEX2 and 4 at 3.16 kHz. These methods were not applied to other parameters as the double plateau phenomena was not clearly present for the remaining parameters.
- **IMP-3 Boundary Redefinition**: IMP-3 utilises the linear correlation between the impedance (represented on a log scale) and the degree of cure for the isothermal region of cure. As the cure cycles utilised in this study were not perfectly isothermal, instead the region was bounded from the global maximum or minimum to the end of the isothermal hold.
- **COND-3 Definition Clarification:** COND-3 originally defined the vitrification point as the start of the plateau region, without providing a clear definition of how to identify the start of the plateau region. Based on the results of the proposed correlations, this point was defined specifically as the tangent point of the endset after the global maximum.
- **COND-4 Boundary Redefinition**: Similar to the redefinition for IMP-3 the boundaries of the equation used in this study were not defined as the isothermal period. Rather, σ_0 was defined as the point of maximum conductivity and σ_∞ was defined as the end of the isothermal temperature region. Further, as the T_g and degree of cure are directly related by the DiBenedetto equation, COND-4 in this study was used to determine the degree of cure progression in accordance with Equation (8) in which the equation is normalised by the actual degree of cure calculated by DSC (α_{DSC}). The rationale for this decision is that the simulated progression of both the T_g and degree of cure made in RAVEN are defined by their DiBenedetto

Table 3
Summary of improvements to the DEA analysis techniques specified in Table 1.

Name	Original Method	Improved Method
DISP-1	First local maximum of $\frac{dD}{dt}$	No change
DISP-2	Plateau onset ($\frac{dD}{dt} = 0$)	Minimum abs(dD/dt)
DISP-3	$\tan\delta = 1$ defined as the crossover point between loss and permittivity	No change
IMP-1	Onset of the first plateau after the minimum value of impedance at 1 kHz	Onset of the first plateau after the minimum value of the impedance, at the frequency it can be most clearly identified (1 kHz or higher)
IMP-2	Onset of the second plateau after the minimum value of impedance at 1 kHz	Onset of the second plateau after the minimum value of the impedance, at the frequency it can be most clearly identified (1 kHz or higher)
IMP-3	Linear regression to determine relationship between log (Impedance) and degree of cure over the isothermal range	Linear regression to determine relationship between log (Impedance) and degree of cure between the global minimum and the end of the isothermal hold
COND-1	Global maximum of the conductivity	No change
COND-2	Inflection after the peak of the conductivity	No change
COND-3	Plateau onset ($\frac{d\sigma}{dt} = 0$)	Plateau onset defined as the tangent point of the endset after the global maximum
COND-4	$T_g = \frac{\log\sigma_0 - \log\sigma_t}{\log\sigma_0 - \log\sigma_\infty} T_{g\infty}$ With the conductivity at the start (σ_0) and end (σ_∞) of the isothermal region, conductivity at time t (σ_t), and the measured glass transition temperature ($T_{g\infty}$)	$\alpha = \frac{\log\sigma_0 - \log\sigma_t}{\log\sigma_0 - \log\sigma_\infty} \alpha_{DSC}$ With the conductivity at the maximum (σ_0), the conductivity at the end of the isothermal region (σ_∞), the conductivity at time t (σ_t), and the measured degree of cure (α_{DSC})
LOSS-1	$\alpha = \frac{\log\varepsilon''_0 - \log\varepsilon''_t}{\log\varepsilon''_0 - \log\varepsilon''_\infty}$ With the loss factor at the start (ε''_0) and end (ε''_∞) of the isothermal region, and the loss factor at time t (ε''_t).	$\alpha = \frac{\log\varepsilon''_0 - \log\varepsilon''_t}{\log\varepsilon''_0 - \log\varepsilon''_\infty} \alpha_{DSC}$ With the loss factor at the maximum (ε''_0), the loss factor at the end of the isothermal region (ε''_∞), the loss factor at time t (ε''_t), and the measured degree of cure (α_{DSC})
VISC-1	Plateau onset ($\frac{d\rho}{dt} = 0$)	Minimum abs(dσ/dt)
VISC-2	$\alpha = \frac{\log\rho_t - \log\rho_{min}}{\log\rho_{max} - \log\rho_{min}} \alpha_m$ With the viscosity at time t (ρ_t), minimum viscosity (ρ_{min}), maximum viscosity (ρ_{max}), and the measured degree of cure (α_m)	See COND-4

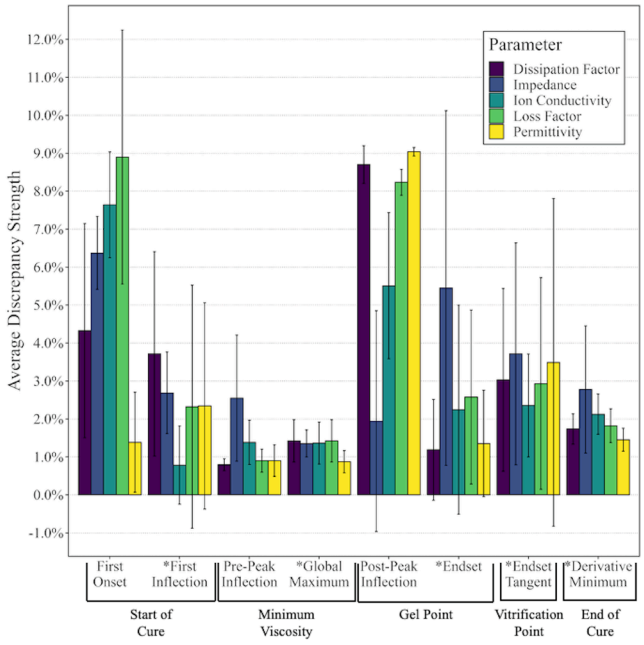

Fig. 6. Results of the cure state identification assessment indicating the average discrepancy strength and standard deviation for each graph feature-cure event pair across all five IDEX replicates.

relationship so the comparison of COND-4 to the simulated degree of cure progression is representative of the relationship and allows for a direct comparison to the other methods which calculate degree of cure (IMP-3, LOSS-1, and VISC-2).

Table 4a
Results comparison for the start of cure.

Time at Cure Start (min)				
	Method	**Average Value**	**Std. Dev**	Δ%
DISP-1 (1 Hz)	*first* $\frac{dD}{dt}$ *maximum*	*56.3*	*5.0*	*1.4%*
Dissipation (100 Hz)	first $\frac{dD}{dt}$ maximum	61.3	5.9	3.4%
Impedance	first $\frac{dZ}{dt}$ minimum	45.4	2.0	2.8%
Ion Conductivity	first $\frac{d\sigma}{dt}$ maximum	51.9	2.7	0.9%
Loss	first $\frac{d\varepsilon''}{dt}$ maximum	56.7	9.2	2.9%
Permittivity	first $\frac{d\varepsilon'}{dt}$ maximum	58.8	7.9	2.9%
RAVEN Predictions	Time at start of cure rate increase (min)	**52.7**	**0.5**	–

Table 4b
Results comparison for the time at minimum viscosity.

Time at Minimum Viscosity (min)				
	Method	**Average Value**	**Std. Dev**	Δ%
COND-1	*Global maximum*	*88.9*	*1.8*	*1.2%*
Dissipation (100 Hz)	Global maximum	88.7	1.4	1.1%
Impedance	Global minimum	88.8	1.8	1.1%
Loss	Global maximum	88.9	1.8	1.2%
Permittivity	Global maximum	87.7	1.3	0.7%
RAVEN Predictions	Time at minimum viscosity (min)	**85.6**	**0.9**	–

Table 4c
Results comparison for the gel point.

Gel Point (min)				
	Method	**Average Value**	**Std. Dev**	Δ%
COND-2	*Post-peak inflection*	*104.0*	*4.4*	*5.4%*
DISP-3 (100 Hz)	*tanδ = 1*	*110.5*	*5.1*	*2.8%*
IMP-1 (1 kHz)	*First endset*	*105.0*	*1.3*	*5.0%*
Dissipation (100 Hz)	Endset	119.6	3.4	1.0%
Impedance	Endset	130.5	10.8	4.9%
Ion Conductivity	Endset	122.4	6.7	2.3%
Loss	Endset	124.9	6.0	2.8%
Permittivity	Endset	116.0	5.5	1.4%
RAVEN Predictions	Time at inflection of viscosity (min)	**117.7**	**1.0**	–

$$\alpha = \frac{\log\sigma_0 - \log\sigma_t}{\log\sigma_0 - \log\sigma_\infty}\alpha_{DSC} \tag{8}$$

- **LOSS-1 Boundary Redefinition**: The calculation for degree of cure defined by LOSS-1 is redefined with the same rationale as COND-4 due to the cure for this study not being truly isothermal. Instead of bounding the start and end of the isothermal region, ε_0'' is defined as the value at the global maximum. Further, the LOSS-1 equation calculates a cure index, which is a relative representation of the degree of cure between values of 0 and 1. This paper normalises the value by the actual degree of cure measured from DSC testing, in the manner of methods COND-2 and VISC-2.

Table 4d
Results comparison for the vitrification point.

Vitrification Point (min)				
	Method	**Average Value**	**Std. Dev**	Δ%
IMP-2 (1 kHz)	*Second endset*	*143.7*	*5.6*	*4.6%*
COND-3	*Flattening of the curve*	*161.3*	*2.1*	*2.2%*
Dissipation (100 Hz)	Endset tangent point	162.2	4.3	2.8%
Impedance	Endset tangent point	165.0	5.6	3.6%
Loss	Endset tangent point	161.3	5.3	3.1%
Permittivity	Endset tangent point	148.9	8.6	3.5%
RAVEN Predictions	Time at Tg-T crossover (min)	**155.6**	**1.4**	–

Table 4e
Results comparison for the end of cure.

Time at Cure End (min)				
	Method	**Average Value**	**Std. Dev**	Δ%
DISP-2 (1 Hz)	$\frac{dD}{dt} = 0$	*N/A*	*N/A*	*N/A*
VISC-1	$\frac{d\rho}{dt} = 0$	*N/A*	*N/A*	*N/A*
Dissipation (100 Hz)	Minimum $\left\|\frac{dD}{dt}\right\|$	250.6	1.8	2.9%
Impedance	Minimum $\left\|\frac{dZ}{dt}\right\|$	245.9	6.4	4.7%
Ion Conductivity	Minimum $\left\|\frac{d\sigma}{dt}\right\|$	248.0	3.3	3.9%
Loss	Minimum $\left\|\frac{d\varepsilon''}{dt}\right\|$	250.4	1.7	2.9%
Permittivity	Minimum $\left\|\frac{d\varepsilon'}{dt}\right\|$	252.2	1.3	2.2%
RAVEN Predictions	Time at end of cure rate (min)	**257.9**	**0.6**	–

- **VISC-1 Redefintion**: VISC-1 identifies the completion of cure as the time where the viscosity derivative reaches zero. However, in this study, the derivatives approach zero but never reach it, as cure is stopped prior to the degree of cure reaching 100%. Instead the correlation will define the end of cure, meaning the point where the cure reaction stops, as the minimum of the absolute value of the deivative.
- **VISC-2 Redefinition**: As the ion conductivity is the inverse of the ion viscosity, COND-4 will be used in place of VISC-2 in order to eliminate redundancy.

3. Results

3.1. Newly proposed cure state identification assessments

The results of the cure point analysis are displayed in Fig. 6. The individual cure events are paired with their proposed graph features in accordance with the x-axis labels. Within each pair grouping, the average discrepancy strength across the replicates of IDEX1-5 as calculated by Equation (7) is displayed for each dielectric parameter. The error bar represents the standard deviation across the part replicates. Note that while the average value is calculated as an absolute value per Equation (7), the standard deviation is calculated based on the true values in order to accurately convey the variance of where t_{DEA} lies relative to t_{RAVEN}.

The pairs with the best consistency and accuracy (indicated in Fig. 6 by asterisks*) are proposed as new correlations: the initial inflection indicating the start of the cure reaction, peak value (global maxima or minima) indicating the point of minimum viscosity, the endset after the global peak indicating the gel point, and the endset tangent point correlating to the vitrification point. These correlations were then compared quantitatively to the existing correlations, shown in Table 4a-e. The existsing correlations in Table 4 are indicated in itallics.

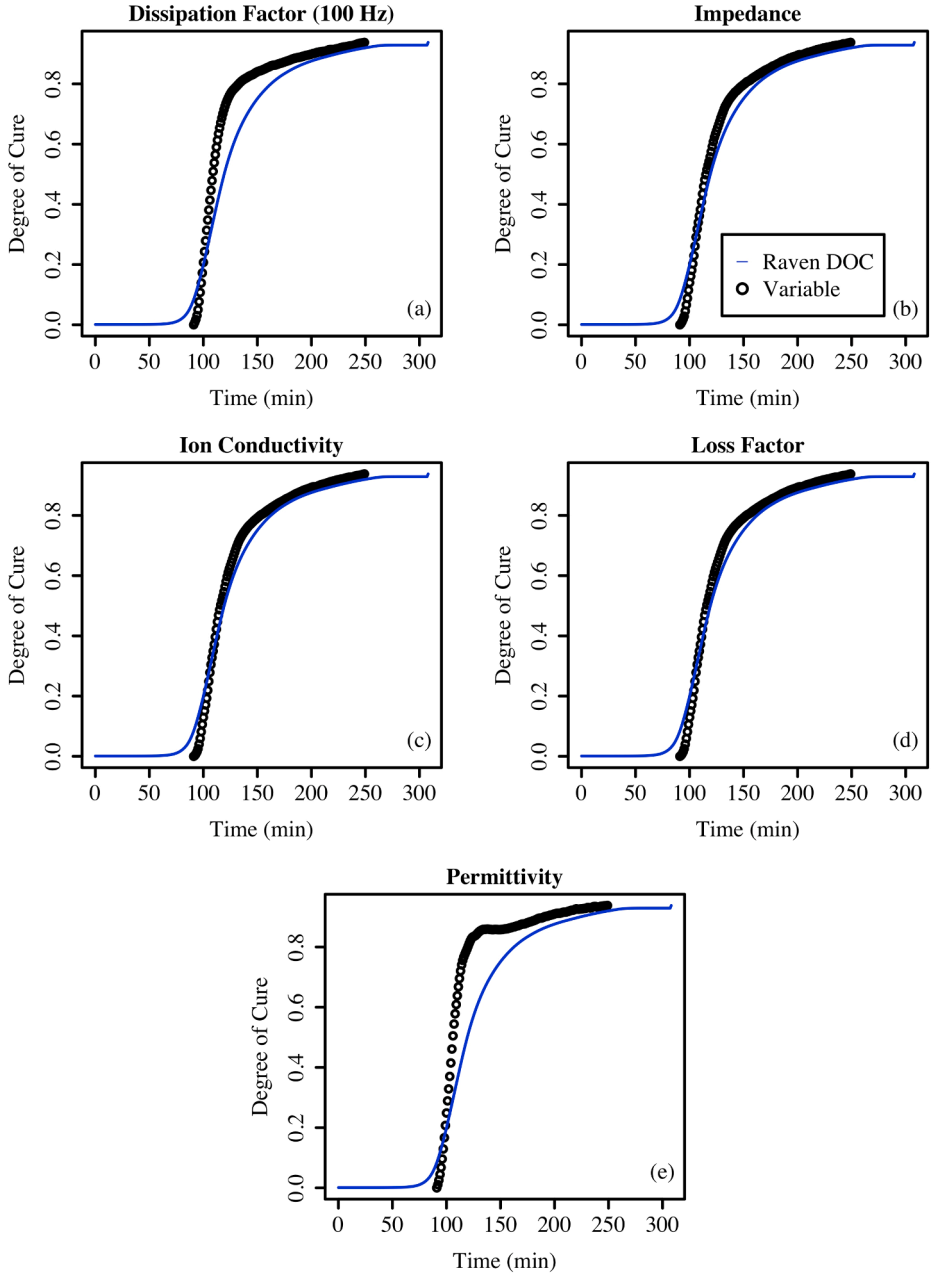

Fig. 7. Calculation of degree of cure for IDEX1 using the (a) dissipation factor at 100 Hz, (b) impedance, (c) ion conductivity, (d) loss factor, and (e) permittivity with all calculations shown in comparison to the RAVEN simulation. Graphs (b-e) represent 1 Hz frequency measurements.

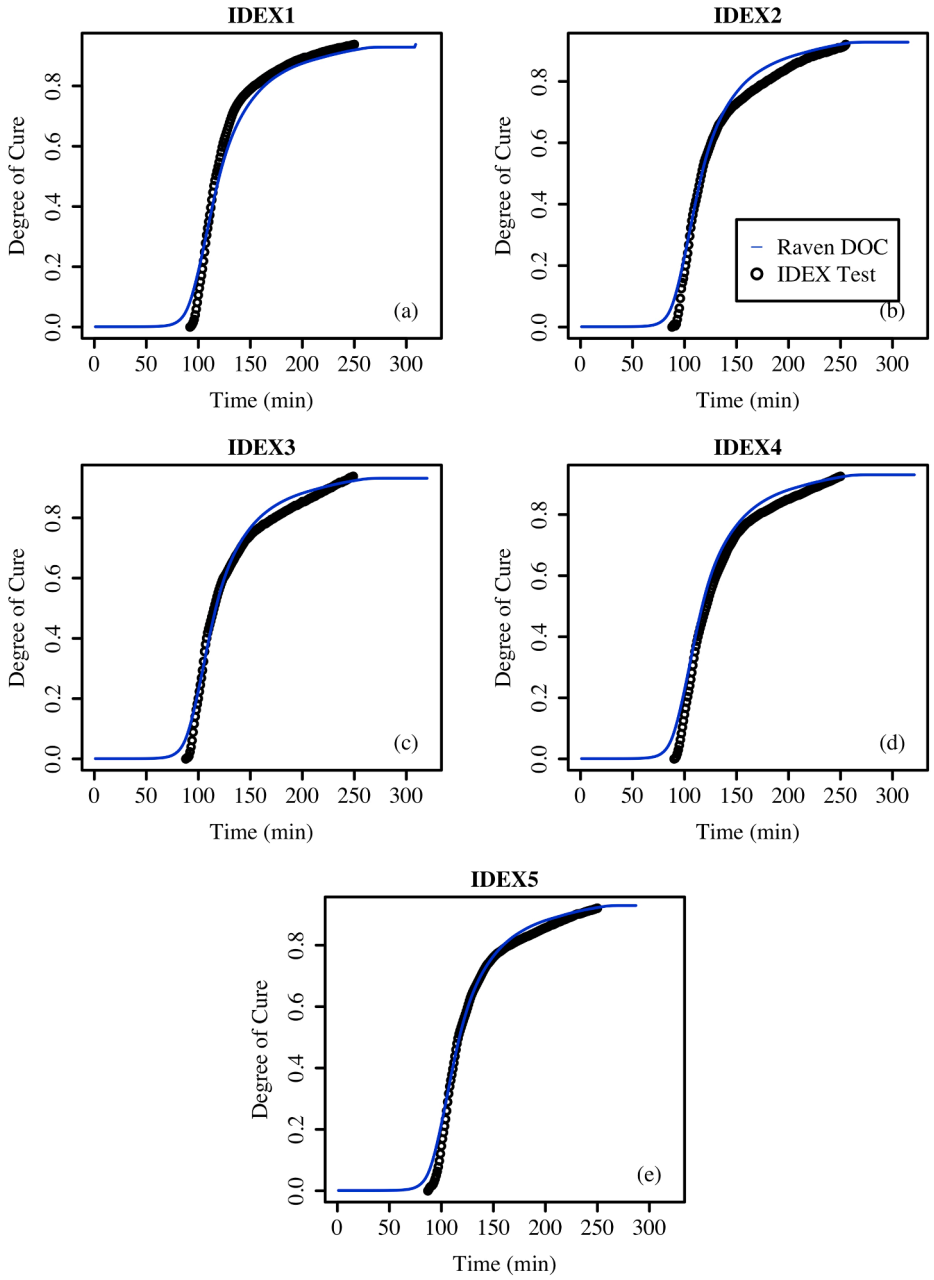

Fig. 8. Comparison of degree of cure calculations via COND-4 (1 Hz) for IDEX tests 1 through 5.

3.2. Accuracy comparisons of different cure state identifications

The results of all proposed and existing correlations which identify discrete cure points are shown in Table 4a-e. For each specified method an average value, standard deviation, and percentage of how closely the value deviates from the RAVEN prediction are presented. The percent discrepancy (Δ%) is calculated in accordance with Equation (7). Note that existing correlations in accordance with Table 3 are indicated in italics.

3.3. Graphical methods

Fig. 7 demonstrates the methods of COND-4 and LOSS-4 applied to all five dielectric parameters for IDEX1. Dielectric correlations are compared to the RAVEN simulated degree of cure. As previously noted, COND-4 is not utilised to calculate the T_g as the T_g and degree of cure are directly related via the DiBenedetto equation. All these correlations were normalised by the actual degree of cure measured by DSC. Further, Fig. 8 displays the part-to-part consistency of COND-4 across the five cure replicates.

The methodology proposed by IMP-3 was applied to all parameters, with the results for IDEX2 shown in Fig. 9 correlations between the RAVEN degree of cure and the parameters are shown in **(a-e)**, including the R^2 value. The linear region was determined from the global maxima or minima to the end of the isothermal dwell, and the correlation function was determined per Equation (9) in which X represents the dielectric parameter, α_{RAVEN} representing the RAVEN calculated degree of cure, and c and b as fitting parameters. The linear equations for each parameter and replicate are given in Table 5.

$$\log X = c\alpha_{RAVEN} + b \tag{9}$$

This equation was then used to calculate a predicted degree of cure

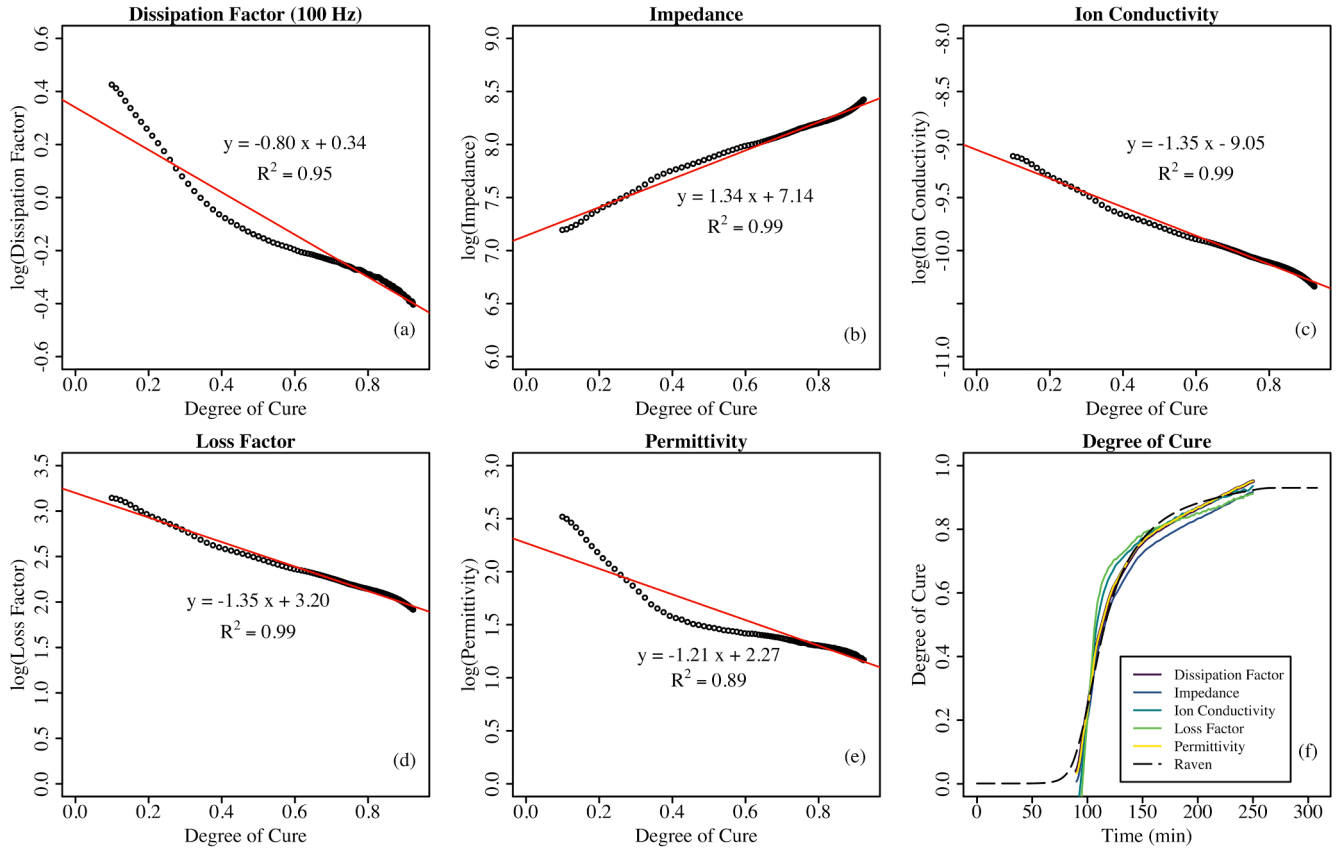

Fig. 9. Linear regression in accordance with IMP-3 for each parameter of IDEX3 indicating the linear relationship between degree of cure and the logarithm of (a) dissipation factor at 100 Hz, (b) impedance, (c) ion conductivity, (d) loss factor, and (e) permittivity. Degree of cure predictions for each parameter compared to the RAVEN simulation are shown in (f). Graphs (b-e) represent 1 Hz frequency measurements.

Table 5
Linear relationships for each dielectric parameter following the method of IMP-3. Note that the 100 Hz correlation for the dissipation factor was used for the degree of cure calculation, and the 1 Hz relationship is only included for the purposes of analysing the slopes.

	IDEX1	IDEX2	IDEX3	IDEX4	IDEX5
Dissipation (100 Hz)	$-1.44D + 0.89$	$-0.82D + 0.33$	$-0.80D + 0.34$	$-0.79D + 0.39$	$-1.26D + 0.81$
Dissipation (1 Hz)	$-0.33D + 0.91$	$-0.39D + 1.12$	$-0.14D + 0.93$	$-0.30D + 0.94$	$-0.22D + 0.86$
Impedance	$2.31Z + 6.43$	$1.46Z + 7.12$	$1.34Z + 7.14$	$1.42Z + 7.05$	$1.94Z + 6.66$
Ion Conductivity	$-2.33\sigma - 8.34$	$-1.47\sigma - 9.03$	$-1.35\sigma - 9.05$	$-1.44\sigma - 8.96$	$-1.95\sigma - 8.57$
Loss Factor	$-2.33\varepsilon' + 3.92$	$-1.47\varepsilon' + 3.23$	$-1.35\varepsilon' + 3.20$	$-1.44\varepsilon' + 3.30$	$-1.95\varepsilon' + 3.68$
Permittivity	$-2.00\varepsilon'' + 3.00$	$-1.08\varepsilon'' + 2.10$	$-1.21\varepsilon'' + 2.27$	$-1.14\varepsilon'' + 2.36$	$-1.73\varepsilon'' + 2.82$

using the actual log values and the fitting parameters. Degree of cure curves for each parameter in IDEX3 are shown in Fig. 9**(f)** in comparison to the RAVEN predicted degree of cure. The final values of this calculation indicate the final degree of cure for each test. These values are compared with actual degree of cure measurements in Table 6.

4. Discussion

4.1. Cure event correlations

Looking first at the cure event correlations determined from Fig. 6 it is apparent the proposed correlations (specified by the asterisks*) are as

Table 6
Predicted degree of cure values as calculated from IMP-3 correlations. Values are compared to analytical results from DSC and DMA and to simulated results from RAVEN.

		IDEX1	IDEX2	IDEX3	IDEX4	IDEX5
Analytical and Simulated Results	**DSC**	93.8%	92.0%	92.8%	92.5%	92.0%
	DMA[a]	93.5%	93.6%	93.2%	93.7%	93.0%
	RAVEN	92.9%	92.8%	93.1%	93.0%	92.9%
DEA Correlations	**Dissipation Factor**	90.4%	90.1%	93.6%	92.7%	89.9%
	Impedance	92.2%	95.0%	95.1%	94.8%	92.2%
	Ion Conductivity	93.3%	95.4%	91.7%	91.2%	92.8%
	Loss Factor	91.0%	91.7%	95.1%	94.3%	92.5%
	Permittivity	87.7%	87.7%	91.3%	94.1%	90.0%

[a] As calculated using the DiBenedetto equation.

good as or better than the existing methods for CYCOM® 5320-1, as demonstrated in the **Table 4** comparisons for each cure event. The discrepancy strengths for the proposed correlations are all within 5%, indicating strong alignment with the RAVEN predictions.

Firstly, there is a weak correlation between the first inflection (also known as the first local $\frac{dX}{dt}$ maximum, in which X represents the relevant dielectric parameter) and the start of cure as proposed in DISP-1 and displayed in Table 4a. At the start of cure the resin has started to soften and lower in mechanical viscosity. This results in a rapid change of the ionic viscosity, which manifests as a rapid increase in the signal. However, the rapid change of temperature during this region has a significant impact on ion viscosity and reduces the accuracy of this correlation. It is proposed that this point may generally indicate that the reaction has started, however the variability should be considered. The ion conductivity measurement, and thus the ion viscosity measurement, have the strongest and most consistent correlations for identifying cure start.

The point of minimum mechanical viscosity, shown in Table 4b, is a key parameter for many manufacturing processes including out of autoclave prepreg processing and resin infusion processing. This time event is very strongly identified as the global maxima or minima of each dielectric parameter, with strong correlations for all tests. COND-1 proposed that the peak value of the ionic conductivity curve has been well identified as the point of maximum ion viscosity. This directly correlates to the point of minimum mechanical viscosity (η) through Equation (10) which is calculated using the ion radius (r), charge (q), and concentration (n) [48]:

$$\rho = \frac{6\pi\eta r}{q^2 n} \tag{10}$$

This study demonstrates that this correlation is valid for all five dielectric parameters as well.

The gel point is challenging to identify, as mechanical gelation occurs over time. There are multiple definitions of gel from the onset of crosslinking to the point of rapid mechanical viscosity increase. Existing correlations such as COND-2 and IMP-1 likely correlate well with the onset of gel, results of which are shown in Table 4c. However, they are less accurate in estimating gel per the definition used by this paper, which is the time at inflection of the mechanical viscosity. DISP-3 correlates well to the gel point and has been shown to relate directly to the crossover point of the storage and loss modulus as calculated in rheology testing [49]. Rather than the inflection point, which was proposed by COND-2, the endset after the global peak correlates strongly to the gel point across all dielectric parameters. At the gel point the resin experiences a rapid increase in the mechanical viscosity, which significantly reduces both ion mobility and dipole movement as the polymer chains rapidly crosslink. As the viscosity curve in Fig. 3**(b)** shows, the inflection point occurs very close in time to the resin achieving maximum viscosity. The endset of the dielectric parameters indicates that the change in electrical signal has rapidly slowed down and suggests a strong alignment to this physical event.

The vitrification point, as defined by the time that the T_g surpasses the processing temperature, is also an arbitrary physical event that is challenging to model with electrical phenomena. As indicated in Table 4d, IMP-2 correlates moderately well for cures of 5320-1, however it is challenging to identify this point at a consistent electrical field excitation frequency. COND-3 was not demonstrated to correlate well for this resin system, and instead applies best to the end of cure, as will be discussed later. The newly proposed endset tangent point aligns strongly for all dielectric parameters. This point is proposed as a clarified definition of the "onset of the plateau region" which has previously been suggested to indicate vitrification. Physically, vitrification indicates the rapid slowing of the cure reaction as the reaction rate becomes diffusion controlled. At this plateau onset, the electrical signal begins a slow leveling out into a linear region. After this point there is no major change to the electrical signal until the cure ends and the lowered processing temperature causes the signal to decline. Thus, we can see that the onset of this plateau region correlates to the onset of the diffusive region of cure during which the crosslinking process is far more subtle.

Finally, by modifying the definitions of DISP-2 and VISC-1 it is possible to identify the end of cure for both curing types across all parameters as shown in Table 4e. As stated previously, the derivative of each signal did not achieve a value of 0. However, all parameters are shown to trend towards 0, until the signal drifts at the end of the cure due to the reduction in temperature. This final point, defined as the minimum of the absolute value of the derivative function ($|\frac{dX}{dt}|_{min}$), has a strong correlation to the end of the cure reaction rate. It should be noted here that literature has previously referred to this as the completion of the cure reaction. This paper will clarify this definition as the stopping of the cure reaction, which is distinct from the cure reaction proceeding to 100% complete. In a typical composite cure, it is unnecessary to achieve 100% conversion, and instead the cure is considered complete once it has reached a specific threshold, for example, at 88.2% for 5320-1 [50]. As none of the cures in this study were progressed to 100% conversion, it is only possible to correlate this point to the end of the cure reaction rate, which occurs when temperature is removed from the system and the reaction rate lacks sufficient energy to proceed. Taking these definitions, the end of the reaction is very reliably identified across the dielectric parameters.

4.2. Graphical methods

The graphical methods of performing dielectric analysis were also demonstrated to be applicable across all parameters. The results of Fig. 7 and indicate that the methods proposed by COND-4, LOSS-1, and VISC-2 apply to the other dielectric parameters. Fig. 8 demonstrates that this method is also consistent from part to part and can thus be used reliably to evaluate the degree of cure and T_g progression. While the permittivity measurement deviated from the RAVEN prediction during the middle portion of the cure, the end stages of cure aligned well.

4.3. Linear analysis (IMP-3) correlation

The linear regression process proposed by IMP-3 carries much promise for predictive cure modelling. For the example presented in Fig. 9 for IDEX 3, showed very strong linear relationships as indicated by high R^2 values. This resulted in the degree of cure trends for the parameters which aligned very closely with the simulated curve. The linear trends for each IDEX replicate, which are displayed in Table 5, also indicate possible patterns which could be used for predictive cure modelling.

Within each test replicate the impedance, conductivity, and loss factor follow a trend of having very closely matching slopes. As all three of these parameters are dependent on the conductance of the material (G) we can determine that this slope may be associated with the conductive behaviour. Similarly, the permittivity is dependent on the capacitive behaviour of the sample. The dissipation factor can be calculated as the ratio of the permittivity to the loss, and written in logarithmic terms Equation (3) can be rewritten using the inverse relationship of resistivity to conductance as follows:

$$\log D = \log\left(\frac{1}{\omega RC}\right) = \log\left(\frac{G}{\omega \mathrm{C}}\right) = \log G - \log C - \log\omega \tag{11}$$

From Equation (11) we can observe that the log of the dissipation factor is defined by the differences in the log of the conductance and capacitance. This pattern is demonstrated by the slopes of the 1 Hz dissipation factor equations, which are almost exactly the difference between the three conductance-based equations (impedance, conductivity, and loss factor) and the capacitive-based equation (permittivity).

It can also be observed that IDEX tests 2, 3, and 4 displayed very consistent slopes within each parameter. Results for IDEX1 and 5

display, however, different trends, which suggest that linear analysis may be sensitive to the natural manufacturing variability from material and process inconsistencies.

In addition to closely aligning to the degree of cure trend, the IMP-3 correlation has also predicted the final degree of cure by identifying the final value predicted by the model. The values indicated in Table 6 show a high degree of accuracy and are on average within 2.5% of the RAVEN predictions.

4.4. Summary of new methods

Based on the results and discussion presented in the previous sections, Table 7 provides a final list of suggested dielectric analysis techniques. The techniques are identified by the cure state feature that they identify, the previously existing techniques that contributed to the methodology, and notes on how the original technique has been modified or improved. Details of the methods are specified in Table 3.

These methods have potential repercussions to live process monitoring techniques and active control systems. The cure event techniques to identify the start of cure, point of minimum viscosity, gel point, and vitrification point can potentially be identified live as the cure progresses. The cure end identification technique is a response to the change in temperature as the process ends and thus cannot be identified until the final dwell temperature has been completed. It is, however, a good point of redundancy against sensors which monitor the processing temperatures and would reinforce that the process step has completed. DoC(2) has the potential for live prediction of cure if a master equation is determined to capture the linear correlation. Such an equation may be material and process-cycle dependent and may need to account for factors which influence signal and cure variation such as materials and temperature uncertainty. DoC(1) must be calculated after the cure has completed, as the equation is dependent on the final value of the signal at the end of the isothermal plateau. For this reason, it is unlikely to provide live monitoring, however it can provide valuable information after the process has completed.

The use of such dielectric analysis methods also has significant implications on quality control systems for high performance applications. Process requirements are commonly validated using indirect methods such as temperature monitoring. Temperature-based methods rely on knowledge of the material cure kinetics and what permissible temperature windows will produce components which meet quality standards.

Table 7
Final list of parameter-independent correlations, including modifications or clarifications of existing correlations.

Analysis Feature	Method	Incorporated Techniques	Notes
DoC (1)	Calculation per VISC-2	COND-4, LOSS-1, VISC-2	Updated to include all parameters
DoC (2)	Linear analysis per IMP-3	IMP-3	Updated to include all parameters
Cure Start	First local maximum of dX/dt	DISP-1	Updated to include all parameters
Viscosity	Global maximum or minimum	COND-1	Updated to include all parameters
Gel Point	Endset after global max/min	COND-2	Modified – applies to all parameters, updated definition due to stronger correlation to endset rather than inflection
Vitrification	Tangent point after endset	COND-3	Modified – applies to all parameters, updated definition of “plateau onset”
Cure End	Minimum of absolute value of dX/dt	DISP-2, VISC-1	Modified - applies to all parameters, updated definition

However, uncertainty in cure kinetics and processing conditions can produce a range of unexpected outcomes [19,51]. By directly monitoring the material state during cure it is possible to objectively identify how the cure progresses for that specific part at that specific time. Dielectric analysis is unique in its ability to directly produce information related to both the stage of cure and final degree of cure, without the required assumptions which predicates temperature monitoring methods.

5. Conclusion

The consistency and accuracy of dielectric analysis has been demonstrated through analysis of multiple part cures. Test results are consistent from part to part and from parameter to parameter, indicating that DEA is capable of reliably identifying material changes throughout the cure process. A comprehensive evaluation of existing and proposed DEA techniques across all dielectric parameters has resulted in the final list of analysis techniques summarised in Table 7. These techniques have been demonstrated to be parameter-independent and to have high degrees of accuracy when compared to analytical and simulated results. Further, correlation methods DISP-3, IMP-1, and IMP-2 have been confirmed to apply to the tests conducted here, however they are parameter-dependent.

The methods evaluated here have implications for live process monitoring and active control, as some methods are capable of providing material state information during the progression of the cure. Further, dielectric analysis has been shown to directly monitor cure state and degree of cure, in contrast to other methods which make assumptions of the material state based on temperature monitoring. This direct monitoring can be used to certify that process conditions are met without concern for process uncertainty or variability.

CRediT authorship contribution statement

Molly Hall: Conceptualization, Methodology, Formal analysis, Investigation, Writing – original draft, Visualization. **Xuesen Zeng:** Writing – review & editing, Supervision, Funding acquisition. **Tristan Shelley:** Writing – review & editing, Supervision. **Peter Schubel:** Writing – review & editing, Supervision, Funding acquisition.

Declaration of Competing Interest

The authors declare that they have no known competing financial interests or personal relationships that could have appeared to influence the work reported in this paper.

Data availability

Data will be made available on request.

References

[1] Alajarmeh O, Zeng X, Aravinthan T, Shelley T, Alhawamdeh M, Mohammed A, et al. Compressive behaviour of hollow box pultruded FRP columns with continuous-wound fibres. Thin-Walled Struct 2021;168:108300.
[2] Alhawamdeh M, Alajarmeh O, Aravinthan T, Shelley T, Schubel P, Mohammed A, et al. Review on local buckling of hollow box FRP profiles in civil structural applications. Polymers (Basel) 2021;13(23):4159.
[3] Brøndsted P, Lilholt H, Lystrup A. Composite materials for wind power turbine blades. Annu Rev Mat Res 2005;35(1):505–38.
[4] Mishnaevsky L, Branner K, Petersen HN, Beauson J, McGugan M, Sorensen BF. Materials for wind turbine blades: an overview. Materials (Basel) 2017;10(11).
[5] Weaver A. Composites drive VT diversification. Reinf Plast 1997;41(1):28–31.
[6] Kim S-Y, Shim CS, Sturtevant C, Kim D, Song HC. Mechanical properties and production quality of hand-layup and vacuum infusion processed hybrid composite materials for GFRP marine structures. Int J Nav Archit Ocean Eng 2014;6(3):723–36.
[7] Mouritz AP, Gellert E, Burchill P, Challis K. Review of advanced composite structures for naval ships and submarines. Compos Struct 2001;53(1):21–42.

[8] Hayman B, Echtermeyer A, McGeorge D. Use of fibre composites in naval ships. 2001.
[9] Kim D-D-W, Hennigan DJ, Beavers KD. Effect of fabrication processes on mechanical properties of glass fiber reinforced polymer composites for 49 meter (160 foot) recreational yachts. Int J Naval Architect Ocean Eng 2010;2(1):45–56.
[10] Feraboli P, Masini A. Development of carbon/epoxy structural components for a high performance vehicle. Compos B Eng 2004;35(4):323–30.
[11] Barile C, Casavola C. Mechanical characterization of carbon fiber reinforced plastics specimens for aerospace applications. Polym Compos 2018;40(2):716–22.
[12] Rocha H, Semprimoschnig C, Nunes JP. Sensors for process and structural health monitoring of aerospace composites: a review. Eng Struct 2021;237:112231.
[13] Mouton S, Teissandier D, Sébastian P, Nadeau JP. Manufacturing requirements in design: The RTM process in aeronautics. Compos A Appl Sci Manuf 2010;41(1):125–30.
[14] Marsh G. Composites - Prime enabler for wind energy. Reinf Plast 2003.
[15] Summerscales J, Searle T. Low-pressure (vacuum infusion) techniques for moulding large composite structures. In: Seminar on Advanced Processes and Manufacture of Composite Structure. Bristol 2005.
[16] Michaud DJ, Beris AN, Dhurjati PS. Thick-sectioned RTM composite manufacturing: Part I – In situ cure model parameter identification and sensing. J Compos Mater 2016;36(10):1175–200.
[17] Tifkitsis KI, Skordos AA. Stochastic multi-objective optimisation of composites manufacturing process. In: Thematic Conference on Uncertainty Quantification in Computational Sciences and Engineering. Rhodes, Island, Greece, 2017. p.690-705.
[18] Michaud DJ, Beris AN, Dhurjati PS. Thick-sectioned RTM composite manufacturing, Part II. Robust cure cycle optimization and control. J Compos Mater 2016;36(10):1201–31.
[19] Mesogitis TS, Skordos AA, Long AC. Stochastic simulation of the influence of cure kinetics uncertainty on composites cure. Compos Sci Technol 2015;110:145–51.
[20] Mesogitis TS, Skordos AA, Long AC. Uncertainty in the manufacturing of fibrous thermosetting composites: a review. Compos A Appl Sci Manuf 2014;57:67–75.
[21] Konstantopoulos S, Hueber C, Antoniadis I, Summerscales J, Schledjewski R. Liquid composite molding reproducibility in real-world production of fiber reinforced polymeric composites: a review of challenges and solutions. Adv Manuf Polym Compos Sci 2019;5(3):85–99.
[22] Ersoy N, Garstka T, Potter K, Wisnom MR, Porter D, Clegg M, et al. Development of the properties of a carbon fibre reinforced thermosetting composite through cure. Compos A Appl Sci Manuf 2010;41(3):401–9.
[23] Pindinelli C, Montagna G, Luprano VAM, Maffezzoli A. Network development during epoxy curing: experimental ultrasonic data and theoretical predictions. Macromol Symp 2002;180(1):73–88.
[24] Lionetto F, Montagna F, Maffezzoli A. Ultrasonic dynamic mechanical analysis of polymers. Appl Rheol 2005;15(5):326–35.
[25] Pommer C, Sinapius M. A Novel approach to monitoring the curing of epoxy in closed tools by use of ultrasonic spectroscopy. Sensors (Basel) 2017;18(1):96.
[26] Rao Y-J. In-fibre Bragg grating sensors. Meas Sci Technol 1997;8(4):355–75.
[27] Lekakou C, Cook S, Deng Y, Ang TW, Reed GT. Optical fibre sensor for monitoring flow and resin curing in composites manufacturing. Compos A Appl Sci Manuf 2006;37(6):934–8.
[28] Grande AM, Di Landro L, Bettini P, Baldi A, Sala G. RTM process monitoring and strain acquisition by fibre optics. Procedia Eng 2011;10:3497–502.
[29] Senturia SD, Sheppard Jr NF. Dielectric Analysis of Thermoset Cure 1985.
[30] Mijović J, Sa A, Fitz B, Zurawsky W, Mondragon I, Bellucci F, et al. Impedance spectroscopy of reactive polymers. 3. Correlations between dielectric, spectroscopic, and rheological properties during cure of a trifunctional epoxy resin. J Polym Sci B 1996;34(2):379–88.
[31] Maistros GM, Partridge IK. Monitoring autoclave cure in commercial carbon fibre/epoxy composites. Compos B Eng 1998;29(3):245–50.
[32] Konstantopoulos S, Fauster E, Schledjewski R. Monitoring the production of FRP composites: a review of in-line sensing methods. Express Polym Lett 2014;8(11):823–40.
[33] Torres M. Parameters' monitoring and in-situ instrumentation for resin transfer moulding: a review. Compos A Appl Sci Manuf 2019;124:105500.
[34] Hall M, Zeng X, Shelley T, Schubel P. In situ thermoset cure sensing: a review of correlation methods. Polymers (Basel) 2022;14(15):2978.
[35] Fournier J, Williams G, Duch C, Aldridge GA. Changes in molecular dynamics during bulk polymerization of an epoxide−amine system as studied by dielectric relaxation spectroscopy. Macromolecules 1996;29(22):7097–107.
[36] Tifkitsis KI, Skordos AA. A novel dielectric sensor for process monitoring of carbon fibre composites manufacture. Compos A Appl Sci Manuf 2019;123:180–9.
[37] Mijovic J, Yee CFW. Use of complex impedance to monitor the progress of reactions in epoxy/amine model systems. Macromolecules 1994;27(25):7287–93.
[38] Steeman PAM, van Turnhout J. A numerical Kramers-Kronig transform for the calculation of dielectric relaxation losses free from Ohmic conduction losses. Colloid Polym Sci 1997;275(2):106–15.
[39] Kratz J, Hsiao K, Fernlund G, Hubert P. Thermal models for MTM45-1 and Cycom 5320 out-of-autoclave prepreg resins. J Compos Mater 2012;47(3):341–52.
[40] Kim D, Centea T, Nutt SR. Out-time effects on cure kinetics and viscosity for an out-of-autoclave (OOA) prepreg: modelling and monitoring. Compos Sci Technol 2014;100:63–9.
[41] ASTM D7028-07(2015), Standard Test Method for Glass Transition Temperature (DMA Tg) of Polymer Matrix Composites by Dynamic Mechanical Analysis (DMA). West Conshohocken, PA: ASTM International; 2015.
[42] Technical Data Sheet CYCOM(R) 5320-1 Prepreg. Solvay Composite Materials.
[43] Day DR, Lewis TJ, Lee HL, Senturia SD. The role of boundary layer capacitance at blocking electrodes in the interpretation of dielectric cure data in adhesives. J Adhes 2006;18(1):73–90.
[44] Kim J-S, Lee DG. On-line cure monitoring and viscosity measurement of carbon fiber epoxy composite materials. J Mater Process Technol 1993;37(1–4):405–16.
[45] Mijovic J, Yee CFW. Use of complex impedance to monitor the progress of reactions in epoxy/amine model systems. Macromolecules 2002;27(25):7287–93.
[46] Yang Y, Plovie B, Chiesura G, Vervust T, Daelemans L, Mogosanu D-E, et al. Fully integrated flexible dielectric monitoring sensor system for real-time in situ prediction of the degree of cure and glass transition temperature of an epoxy resin. IEEE Trans Instrum Meas 2021;70:1–9.
[47] Kim SS, Murayama H, Kageyama K, Uzawa K, Kanai M. Study on the curing process for carbon/epoxy composites to reduce thermal residual stress. Compos A Appl Sci Manuf 2012;43(8):1197–202.
[48] Boll D, Schubert K, Brauner C, Lang W. Miniaturized flexible interdigital sensor for *in situ* dielectric cure monitoring of composite materials. IEEE Sens J 2014;14(7):2193–7.
[49] Chaloupka A, Pflock T, Horny R, Rudolph N, Horn SR. Dielectric and rheological study of the molecular dynamics during the cure of an epoxy resin. J Polym Sci B 2018;56(12):907–13.
[50] Bruk D. Implementation Methodology, Validation, and Augmentation of a Cure Kinetic Model for Carbon Fiber/CYCOM 5320-1, FM309-1, and FM300-2 [Doctoral thesis]: Washington University in St. Louis; 2021.
[51] Mesogitis TS, Skordos AA, Long AC. Stochastic heat transfer simulation of the cure of advanced composites. J Compos Mater 2016;50(21):2971–86.
[52] Kazilas MC, Partridge IK. Exploring equivalence of information from dielectric and calorimetric measurements of thermoset cure—a model for the relationship between curing temperature, degree of cure and electrical impedance. Polymer 2005;46(16):5868–78.
[53] O'Dwyer MJ, Maistros GM, James SW, Tatam RP, Partridge IK. Relating the state of cure to the real-time internal strain development in a curing composite using in-fibre Bragg gratings and dielectric sensors. Meas Sci Technol 1998;9(8):1153–8.
[54] Hardis R, Jessop JLP, Peters FE, Kessler MR. Cure kinetics characterization and monitoring of an epoxy resin using DSC, Raman spectroscopy, and DEA. Compos A Appl Sci Manuf 2013;49:100–8.
[55] Kahali Moghaddam M, Breede A, Chaloupka A, Bödecker A, Habben C, Meyer E-M, et al. Design, fabrication and embedding of microscale interdigital sensors for real-time cure monitoring during composite manufacturing. Sens Actuat. A 2016;243:123–33.